Science Journal of Chemistry
2021; 9(2): 29-44
http://www.sciencepublishinggroup.com/j/sjc
doi: 10.11648/j.sjc.20210902.11
ISSN: 2330-0981 (Print); ISSN: 2330-099X (Online)

Synthesis, Characterization, Crystal Structure and Quantum Chemical Calculations of 2-oxo-2H-chromen-3-yl Acetate

Akoun Abou[1, *], Siaka Sosso[2], Affiba Florance Kouassi[3], Thouakesseh Jeremie Zoueu[1], Abdoulaye Djande[2], Olivier Ouari[4]

[1]Department of Training and Research in Electrical and Electronic Engineering, Research Team: Instrumentation, Image and Spectroscopy, Félix Houphouët-Boigny National Polytechnic Institute, Yamoussoukro, Côte d'Ivoire

[2]Department of Chemistry, Laboratory of Molecular Chemistry and Materials, Research Team: Organic Chemistry and Phytochemistry, University Joseph KI-ZERBO, Ouagadougou, Burkina Faso

[3]Department of Physics, Laboratory of Fundamental and Applied Physics, University of Abobo Adjamé—Nangui Abrogoua, Abidjan, Côte d'Ivoire

[4]Department of Chemistry, Radical Chemistry Institute, Research Team SREP, Aix-Marseille University, Marseille, France

Email address:

abouakoun@gmail.com (A. Abou), sossosiaka@yahoo.fr (S. Sosso), akouassi859@yahoo.com (A. F. Kouassi), jzoueu@gmail.com (T. J. Zoueu), djandeabdou@yahoo.fr (A. Djande), olivier.ouari@univ-amu.fr (O. Ouari)

[*]Corresponding author

To cite this article:

Akoun Abou, Siaka Sosso, Affiba Florance Kouassi, Thouakesseh Jeremie Zoueu, Abdoulaye Djande, Olivier Ouari. Synthesis, Characterization, Crystal Structure and Quantum Chemical Calculations of 2-oxo-2H-chromen-3-yl Acetate. *Science Journal of Chemistry*. Vol. 9, No. 2, 2021, pp. 29-44. doi: 10.11648/j.sjc.20210902.11

Received: March 14, 2021; **Accepted**: April 6, 2021; **Published**: April 16, 2021

Abstract: This paper is focused on a combined experimental and theoretical study of 3-substituted coumarin derivative, the 2-oxo-2H-chromen-3-yl acetate (I). The compound was synthesized by reacting chroman-2,3-dione and acetic anhydride in dried diethyl ether in the presence of dried pyridine and crystallized in the orthorhombic crystal system with Pbca space group. The lattice parameters of the structure are a=14.6770 (1), b=7.1079 (1), c=17.6767 (2) Å, α=β=γ=90° with 8 molecules per unit cell (Z=8). The compound has been characterized structurally by Spectroscopy utilizing ^{1}H NMR, ^{13}C NMR and IR techniques and by crystallography using the X-Ray diffraction (XRD) analysis. In the crystallographic study, the positions of the atoms were determined by direct methods and refined to a final R value of 0.038 for 1768 independent reflections. The stabilization of the structure is provided by intermolecular C-H···O hydrogen bonds extending along [010] direction. Likewise, the presence and nature of intermolecular contacts are determined by the 3-D molecular Hirshfeld surface and 2-D fingerprint plot analysis which indicate the main contributions to the Hirshfeld surface, 38.7% for O ··· H and 28.7% for H ·· H. Moreover, the molecular geometry of (I) was as well minimized utilizing density functional theory (DFT/RB3LYP), the frequency calculations with RB3LYP method, the basic *ab initio* model i.e the restricted Hartree-Fock (RHF) and the exchange component of Perdew and Wang's 1991 functional B3PW91 methods with the 6-311^{++}G(d, p) basis set in ground state. The derived structural parameters highlight very good correlation with the crystallographic results. Frontier molecular orbitals (HOMO-LUMO), their energy gap, the non-linear optical effects (NLO) and related reactive parameters were also computed to better apprehend the properties of the molecule.

Keywords: 3-substituted Coumarin Derivative, C—H…O Hydrogen Bonds, Hirshfeld Surface Analysis, Quantum Chemical Computations, Crystal Structure

1. Introduction

Coumarin derivatives are of huge interest as useful materials and have attracted more and more attention nowadays because of their widespread biological properties covering anti-HIV [1, 2], anti-coagulant [3], anti-oxidant [4], anti-tumor [5], anti-bacterial [6], and anti-inflammatory [7].

Given their importance and as an extension of our work on the analysis of the crystal structure of coumarin derivatives [8-9], we report here the synthesis, the crystal structure, the geometry optimization and the Hirshfeld surface analysis of the title compound (I).

2 Experimental and Theoretical Methods

2.1. Synthesis

In a 100 ml round-necked flask topped with a water condenser were introduced successively: dried diethyl ether (25 mL), acetic anhydride (0.65 mL; 6.17 mmol) and dried pyridine (2.35 mL; 4.7 molar equivalents). While stirring strongly, chroman-2,3-dione (1g; 6.17 mmol) was added in small portions over 30 min. The reaction mixture was left under agitation at room temperature for 3 h. The mixture was then poured in a separating funnel containing 40 mL of chloroform and washed with diluted hydrochloric acid solution until the pH was 2–3. The organic phase was extracted, washed with water to neutrality, dried over $MgSO_4$ and the solvent removed. The resulting precipitate was filtered off with suction, washed with petroleum ether and recrystallized from chloroform to obtain yellow laminar crystals of the title compound (I): yield 72%; M.pt. 371-373 K.

2.2. Electrospray Ionisation Mass Spectrum

The analyses were carried out with a 3200 QTRAP spectrometer (Applied Biosystems SCIEX) equipped with a pneumatically assisted air pressure ionization (API) source for ESI-MS^+ experiment. The sample in solution was ionized in the following conditions: electrospray tension (ISV): 5500 V; orifice tension (OR): 20 V; nebulizing gas pressure (air): 10 psi. The mass spectrum (figure 2) was obtained with a quadrupole analyzer.

2.3. IR Spectrum

The infrared spectrum (Figure 3), was run on a Bruker IFS 66/S Fourier Transform Infrared Spectrometer (FT-IR), utilizing the ATR (Attenuated Total Reflectance) technique. The sample (powder or crystal) was directly placed on a germanium crystal and the spectrum was obtained using a detector (MCT). The absorption bands are expressed in wavenumber (cm^{-1}) with a resolution of 1 cm^{-1}.

2.4. ^1H and ^{13}C Spectra

^1H and ^{13}C-NMR spectra (figures 4 and 5) were recorded on a Bruker AMX-400 spectrometer at 400 and 100 MHz respectively, using TMS as internal standard (chemical shifts in δ ppm, J in Hz) and DMSO-d6 as solvent.

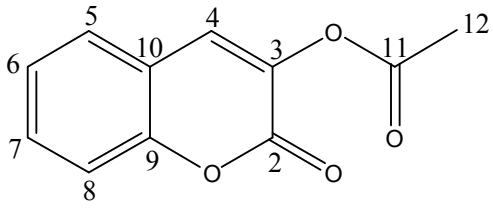

Figure 1. *Atomic numbering scheme for analyzing spectra.*

2.5. Crystal structure Analysis

Diffraction data were gathering using a Rigaku Oxford Diffraction SuperNova, Dual, Cu at zero, AtlasS2 diffractometer [10] utilizing a mirror monochromator and Cu *K*α radiation (λ=1.54184 Å) at 298 K. The raw structure was determined by direct methods with SIR2014 [11] incorporated in the WinGX [12] package. The refinement was performed by full-matrix least squares method on the positional and anisotropic temperature parameters of the non-hydrogen atoms utilizing 137 crystallographic parameters with SHELXL2014 program [13]. All H atoms were geometrically optimized [C—H=0.93 (aromatic), 0.96 Å (methyl)] and refined as riding model approximation with Uiso (H) constrained to 1.2 (aromatic group) or 1.5 (methyl group) times Ueq of the respective parent atom. Data gathering, cell refinement and data reduction are by CrysAlis PRO [10]. The general-purpose crystallographic tool PLATON [14] was used for the structure analysis and presentation of the results. Information on the data gathering conditions and the parameters of the refinement process are summarized in Table 1.

2.6. Hirshfeld Surface

The Hirshfeld surface analysis is a reliable tool to examine intermolecular associations of the molecules in a crystal packing. This tool implemented in Crystal Explorer 3.1 software [15] is used in this work to compute Hirshfeld surfaces map and 2-D fingerprint plots of 2-oxo-2H-chromen-3-yl acetate with a standard (high) surface resolution.

2.7. Computational Procedures

The geometry optimization of compound (I) was computed employing the density functional theory (DFT) and the frequency calculations both using restricted RB3LYP exchange correlation functional, the restricted Hartree-Fock (RHF) and the exchange component of Perdew and Wang's 1991 functional B3PW91 methods. The four methods were performed with the GAUSSIAN09 program package [16] utilizing the structure originating from crystallographic study as the starting structure for the computations. Further, 6-311^{++}G (d, p) basis set is applied to all calculation methods.

3. Results and Discussion

3.1. Spectra Analysis

3.1.1. Electrospray Ionisation Mass Spectrum

In the mass spectrum (figure 2), the peaks detected at *m/z* *205*, *222* and *227* due to the pseudo-molecular ion $[M+H]^+$, the ammonium adduct $[M+NH_4]^+$ and the sodium adduct $[M+Na]^+$ successively, confirmed the molecular weight of 204 $g.mol^{-1}$ which is in accordance with the chemical formula $C_{11}H_8O_4$. The black dot observe in the spectrum indicates an ion that is not specific to the sample.

3.1.2. Infrared (FT-IR) Spectrum

The FT-IR spectrum of compound I (figure 3) highlighted the main characteristic absorption bands: 1776.7 cm^{-1} (C=O, ester); 1731.8 cm^{-1} (C=O, lactone); 1189.8 cm^{-1} (C-O, ester); 1081.7 cm^{-1} (C-O, lactone); 3064 cm^{-1} (C-H, aromatic) and 1607.4 cm^{-1} (C=C, aromatic).

3.1.3. ^{1}H-NMR Spectrum

The analysis (chemical shifts and coupling constants) of the ^{1}H NMR spectrum (figures 4) showed six signals with five in the range 6-8.5 ppm due to aromatic hydrogens, the three equivalent methyl protons appeared unambiguously at 2.49 ppm.

^{1}H-NMR (DMSO-d6, 400 MHz, δ ppm): 8.00 (s, 1H, H-4); 7.72 (dd, 1H, *J*=8.0, 2.1 Hz, H-5); 7.39 (td, 1H, *J*=8.0, 2.0 Hz, H-6); 7.62 (td, 1H, *J*=8.0, 2.1 Hz, H-7); 7.46 (d, 1H, *J*=8.0 Hz, H-8); 2.49 (s, 3H, H-12).

3.1.4. ^{13}C-NMR Spectrum

As expected, eleven peaks were observed in the ^{13}C NMR spectrum (figure 5).

^{13}C-NMR (DMSO-d6, 100 MHz, δ ppm): 156.08 (C-2), 135.33 (C-3), 125.04 (C-4), 131.47 (C-5), 128.44 (C-6), 131.68 (C-7), 116.16 (C-8), 151.52 (C-9), 118.27 (C-10), 168.19 (C-11), 20.12 (C-12).

3.1.5. DEPT-135 Spectrum

The spectrum of compound (I) (Figure 6) showed six positive peaks suggesting the five aromatic tertiary carbons and the shielded primary carbon of methyl group. It is also interesting to note that quaternary carbons (C-2, C-3, C-9, C-10 and C-11) disappeared.

^{13}C (DEPT-135)-NMR (DMSO-d6, 100 MHz, δ ppm): 125.04 (C-4), 131.47 (C-5), 128.44 (C-6), 131.68 (C-7), 116.16 (C-8), 20.12 (C-12).

3.1.6. Conclusion of Spectra Analysis

The overlaying of the spectrometric outcomes originating from the spectral analysis validates the depicted coumarin molecule in Figure 1.

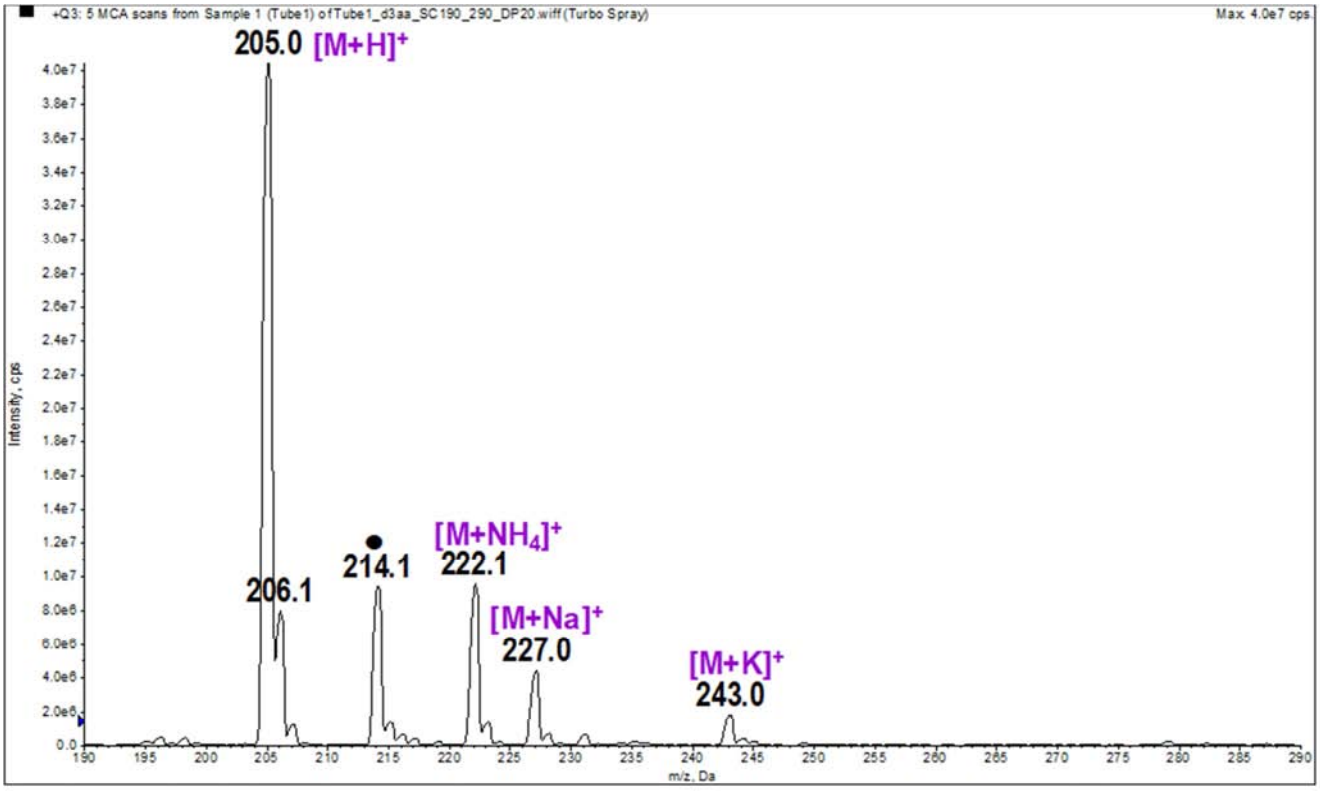

Figure 2. *Experimental ESI-MS spectrum.*

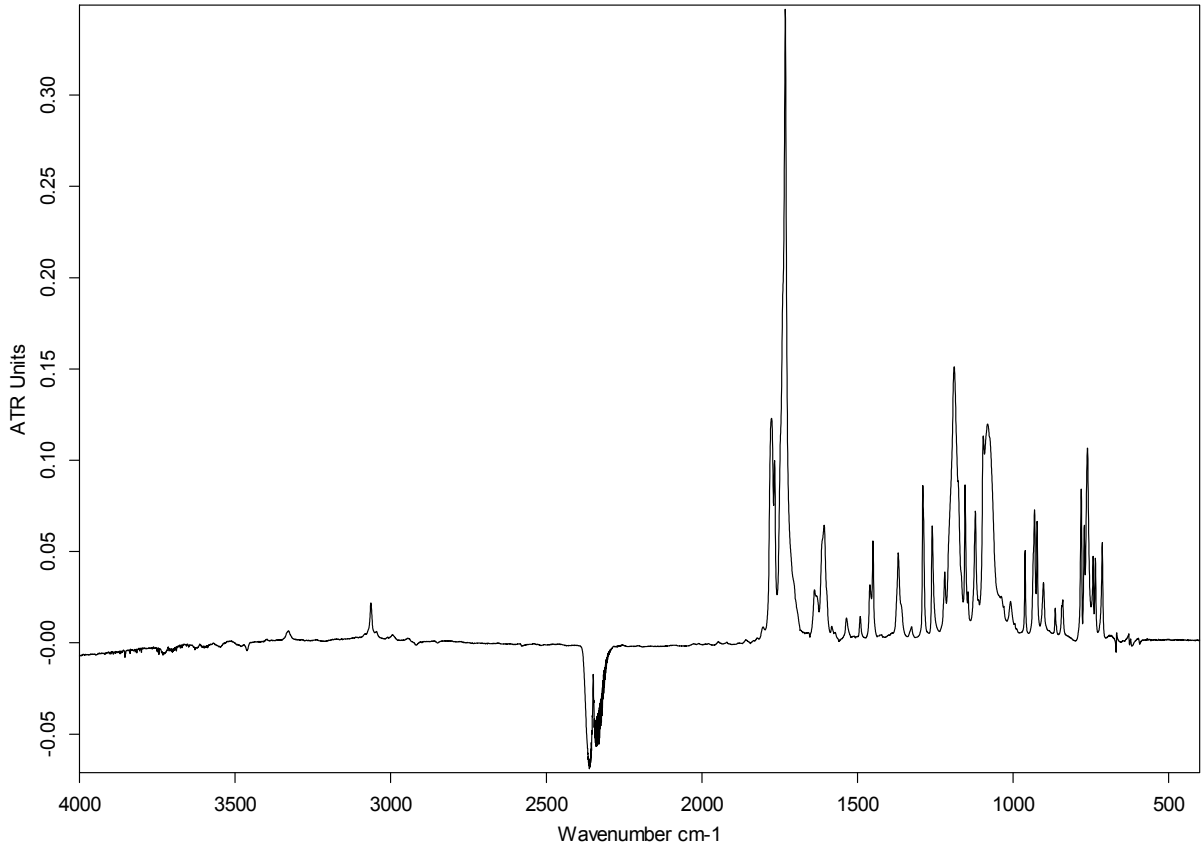

Figure 3. *Experimental FT-IR spectrum.*

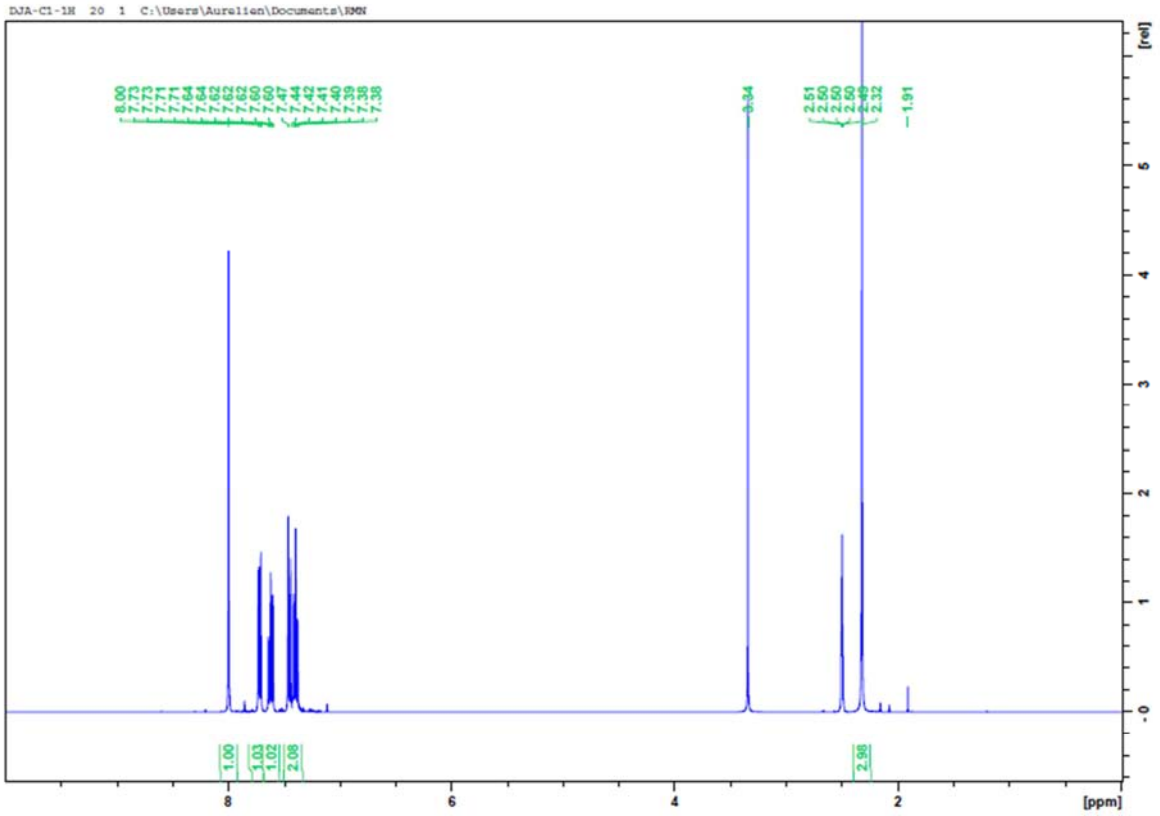

Figure 4. *Experimental ^{1}H-NMR Spectrum.*

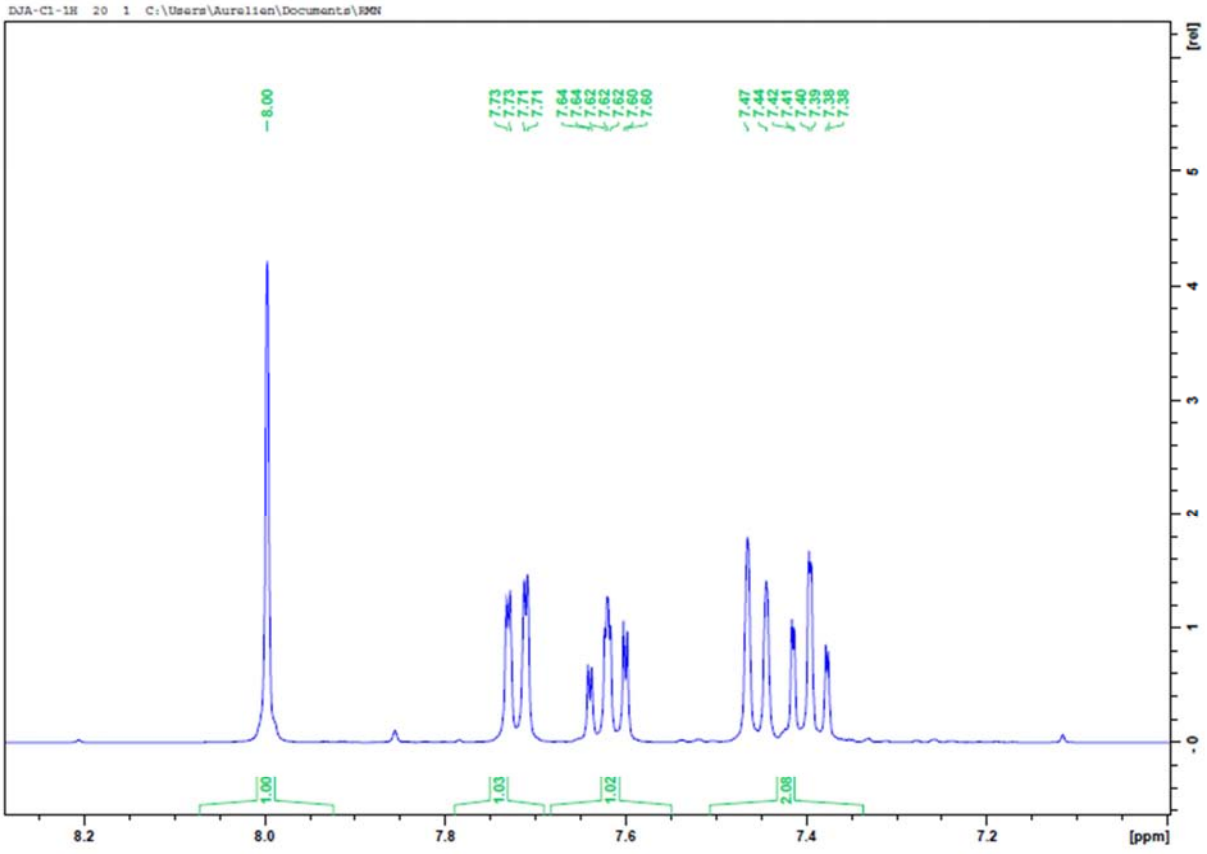

Figure 5. *Experimental [1]H-NMR Spectrum: enlargement of aromatic ring.*

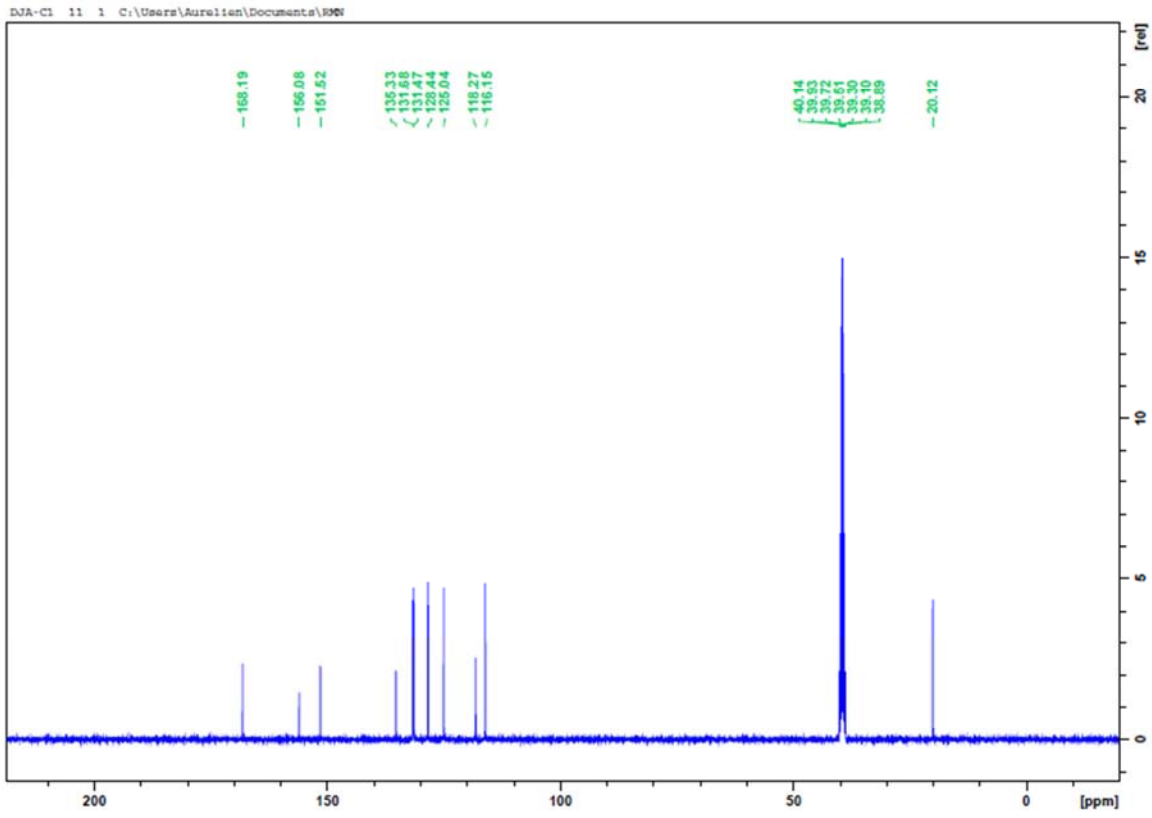

Figure 6. *Experimental [13]C-NMR Spectrum.*

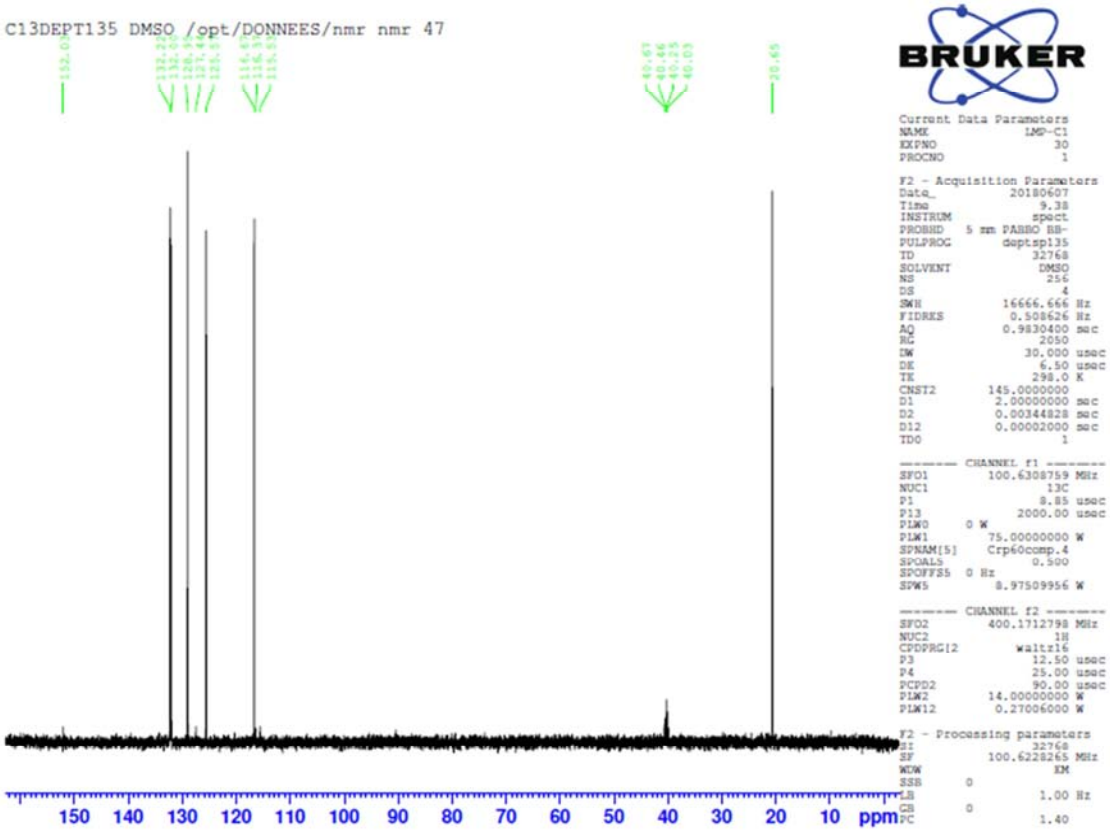

Figure 7. *Experimental DEPT-135 Spectrum.*

3.2. Structural Description

The molecular structure of (I) is represented in Figure 7.

3.2.1. Geometry and Conformation

The positional parameters, bond distances, bond angles and torsion angles are summarized in Tables 3, 4, 5 and 6. The analysis of the geometrical parameters are based on the comparison of these parameters with those from standard values [17]. The results of the investigation reveal their good compliance with the expected standard values despite the slight asymmetry found in the electronic distribution of the pyrone ring generating C2-C3 [1.334 (2) Å] and C1-C2 [1.461 (2) Å] bond distances less and greater respectively than those expected for Car—Car bond. This demonstrates that the electron density is primarily situated in the C2—C3 bond of the pyrone ring, as observed in other coumarin derivatives [18, 19].

Table 1. *Crystal data and details of the structure determination.*

chemical formula	**$C_{11}H_8O_4$**	**Theta range for data collection [°]**	**4.979 - 70.901**
Formula weight	204.17	Crystal size [mm^3]	0.33× 0.14 × 0.06
Temperature [K]	298	Index ranges	-17 ≤ h ≤17; -8 ≤ k ≤ 8; -21 ≤ l ≤ 20
Wavelength λ [Å]	1.54184	Refections collected	18587
Crystal system	Orthorhombic	Absorption coefficient [mm^{-1}]	0.96
Space group	Pbca	Theta full [°]	67.684
Unit cell dimensions		F(000)	848
a [Å]	14.6770 (1)	Refinement method	Full-matrix least squares on F^2
b [Å]	7.1079 (1)	Data/restraints/parameters	1667 /0/ 137
c [Å]	17.6767 (2)	Goodness of fit	1.07
α [°]	90	Final R indices [$F^2 > 2.0\ \sigma(F^2)$]	R_1=0.038, wR_1=0.116
β [°]	90	Density calculated [$g.cm^{-3}$]	1.471
γ [°]	90	Independent reflections	1768
Volume [$Å^3$]	1844.08 (4)	R_{int}	0.028
Z	8	R indices (all data)	0.0395
Crystal description-crystal colour	Prism Yellow	$\Delta\rho_{max}$, $\Delta\rho_{min}$ (e $Å^{-3}$)	0.23, -0.17
Extinction correction:	None	$(\Delta/\sigma)_{max}$	< 0.001
Diffractometer	SuperNova, Dual, Cu at zero, AtlasS2	Absorption correction	multi-scan; CrysAlisPro 1.171.38.43 (Rigaku Oxford Diffraction, 2015) Empirical absorption correction using spherical harmonics, implemented in SCALE3 ABSPACK scaling algorithm.

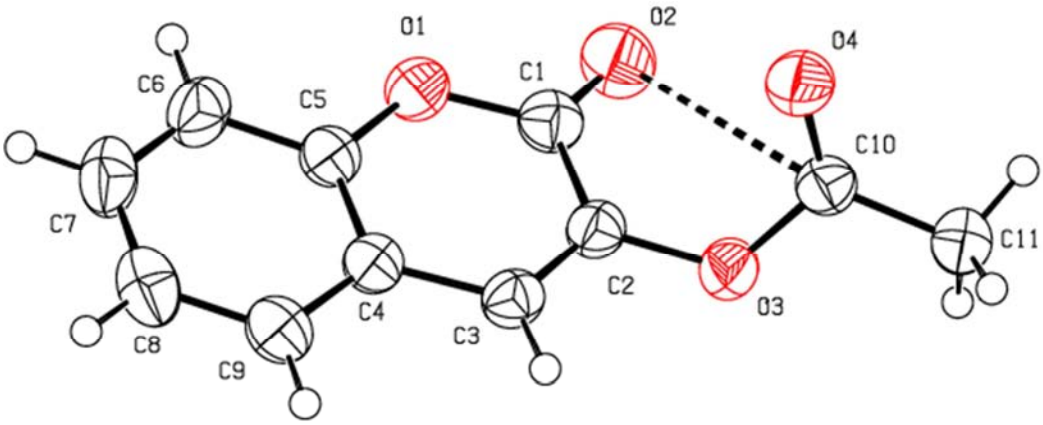

Figure 8. *An ORTEP [12] view of (I) with Atomic numbering scheme. Dashed lines denotes short intramolecular contact.*

In compound (I), the coumarin moiety is planar (r.m.s deviation=0.037 Å) and makes an angle of 22.05 (6)° with respect to the pseudo five membered O2C1C2O3C10 ring established by the short intramolecular O2…C10=3.1385 (15) Å contact (figure 8). The conformation of this pseudo five-membered ring is an envelope as judged by the Puckering parameters (Q=0.6405 (12) Å and Φ=319.00 (11)°) [20]. The resulting tricycle compound is not coplanar as demonstrated by the angle between the coumrin moiety and the pseudo five-membered ring (22.05 (6)°).

3.2.2. Supramolecular Features

In the crystal, C11—H11C…O3 hydrogen bonds (table 2) connect adjacent molecules in an infinite chain along [010] direction (Figure 9). In addition, Platon [14] analysis reveals short contacts [H11A…O2 (1/2-x, -1/2+y, z)=2.65 Å] and [C2…2 (-x,2-y, -z)=3.2313 (16) Å] with distances less than the sum of the van der Waals radii which insure the stability of compound (I).

Table 2. *Hydrogen-bond geometry (Å, °).*

D—H…A	D—H	H…A	D…A	D—H…A
C11—H11C…O3^{i}	0.96	2.59	3.441 (2)	147.9
Symmetry code: (i) −*x*+1/2, *y*+1/2, *z*				

Table 3. *Fractional atomic coordinates and isotropic or equivalent isotropic displacement parameters (Å^2).*

Atom	x	y	z	U_{iso}*/U_{eq}
O3	0.36063 (6)	0.49673 (12)	0.00918 (5)	0.0421 (3)
O1	0.53198 (6)	0.67749 (11)	0.13964 (5)	0.0438 (3)
C5	0.56346 (8)	0.51317 (16)	0.17179 (7)	0.0386 (3)
C4	0.52874 (7)	0.33942 (16)	0.15009 (7)	0.0369 (3)
C6	0.63015 (9)	0.5293 (2)	0.22686 (8)	0.0492 (3)
H6	0.6521	0.6469	0.2411	0.059*
O2	0.44319 (7)	0.82796 (13)	0.05919 (6)	0.0568 (3)
C11	0.21573 (9)	0.55735 (19)	−0.04229 (8)	0.0485 (3)
C7	0.66341 (9)	0.3678 (2)	0.26024 (8)	0.0535 (4)
C9	0.56541 (8)	0.17779 (18)	0.18333 (8)	0.0454 (3)
H9	0.5447	0.0597	0.1685	0.054*
C3	0.45608 (8)	0.33576 (16)	0.09554 (7)	0.0379 (3)
H3	0.4309	0.2217	0.0803	0.046*
C1	0.46416 (8)	0.67976 (17)	0.08623 (7)	0.0406 (3)
C10	0.27554 (8)	0.56698 (16)	0.02550 (7)	0.0390 (3)
C2	0.42497 (8)	0.49711 (16)	0.06687 (6)	0.0368 (3)
O4	0.25572 (6)	0.62334 (14)	0.08671 (5)	0.0538 (3)
C8	0.63196 (9)	0.1926 (2)	0.23786 (8)	0.0521 (4)
H8	0.6560	0.0844	0.2598	0.062*
H7	0.7073	0.3767	0.2981	0.064*
H11A	0.1792	0.4454	−0.0400	0.073*
H11B	0.2526	0.5546	−0.0871	0.073*
H11C	0.1767	0.6657	−0.0435	0.073*

Table 4. *Experimental and calculated bond lengths with 6-311^{++}G(d,p) basis set (Å).*

Bond	X-Ray	DFT/RB3LYP/	FREQ/RB3LYP	HF	B3PW91
O3—C10	1.3756 (14)	1.3879	1.3757	1.3522	1.3818
O3—C2	1.3899 (14)	1.3783	1.3898	1.3612	1.3721
O1—C1	1.3719 (15)	1.3836	1.3724	1.3411	1.3767
O1—C5	1.3787 (15)	1.3677	1.3789	1.3550	1.3612
C3—C2	1.3343 (16)	1.3455	1.3339	1.3223	1.3445
C3—C4	1.4380 (16)	1.4392	1.4375	1.4524	1.4357
O2—C1	1.1970 (15)	1.2005	1.1965	1.1769	1.1991
C4—C5	1.3899 (16)	1.4043	1.3903	1.3849	1.4020
C4—C9	1.3982 (17)	1.4060	1.3987	1.3944	1.4034
O4—C10	1.1899 (15)	1.1964	1.1900	1.1757	1.1952
C2—C1	1.4606 (16)	1.4694	1.4612	1.4765	1.4664
C5—C6	1.3852 (18)	1.4060	1.3850	1.3839	1.3908
C9—C8	1.3762 (19)	1.3855	1.3758	1.3773	1.3833
C6—C7	1.380 (2)	1.3855	1.3799	1.3795	1.3863
C10—C11	1.4870 (17)	1.4997	1.4877	1.4974	1.4946
C8—C7	1.386 (2)	1.4011	1.3855	1.3925	1.3986

Table 5. *Experimental and computed bond angles with 6-311^{++}G(d,p) basis set (°).*

Bond angle	X-Ray	DFT/RB3LYP	FREQ/ RB3LYP	RHF	B3PW91
C10—O3—C2	117.53 (9)	117.14	117.52	118.09	116.61
C1—O1—C5	122.46 (9)	123.37	122.47	124.10	123.38
C2—C3—C4	119.52 (10)	120.16	119.57	119.76	120.01
C5—C4—C9	118.23 (11)	118.41	118.18	118.71	118.46
C5—C4—C3	118.23 (10)	117.71	118.25	117.54	117.68
C9—C4—C3	123.54 (11)	123.87	123.56	123.75	123.86
C3—C2—O3	120.62 (10)	121.72	120.69	122.76	121.82
C3—C2—C1	122.71 (11)	122.35	122.68	121.81	122.29
O3—C2—C1	116.18 (10)	115.78	116.13	115.34	115.73
O1—C5—C6	117.15 (11)	117.40	117.19	117.41	117.34
O1—C5—C4	121.07 (11)	121.11	121.04	121.02	121.24
C6—C5—C4	121.78 (11)	121.49	121.77	121.57	121.42
O2—C1—O1	118.14 (11)	119.11	118.12	120.13	119.17
O2—C1—C2	125.97 (12)	125.61	126.01	124.10	125.45
O1—C1—C2	115.88 (10)	115.26	115.86	115.76	115.37
C8—C9—C4	120.32 (12)	120.52	120.35	120.47	120.53
C7—C6—C5	118.79 (12)	118.97	118.81	118.83	118.99
O4—C10—O3	122.34 (11)	122.48	122.36	122.57	122.44
O4—C10—C11	127.15 (11)	127.42	127.15	126.74	127.40
O3—C10—C11	110.50 (10)	110.10	110.48	110.68	110.15
C9—C8—C7	120.32 (12)	120.68	120.32	119.71	119.91

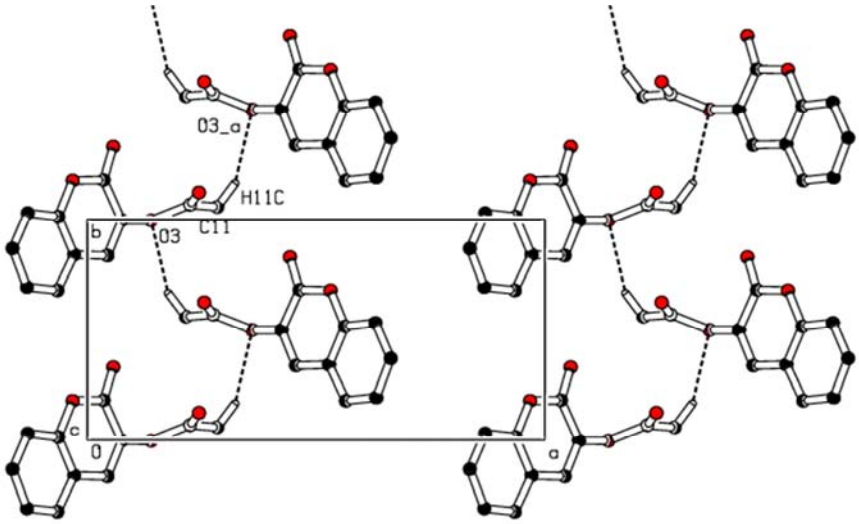

Figure 9. *Part of the crystal packing showing hydrogen bonds (dashed lines) along [010]. H atoms not involved in hydrogen bonding have been omitted for clarity.*

Table 6. *Experimental and computed torsion angles with 6-311^{++}G(d,p) basis set (°).*

Torsion angle	X-ray	DFT/RB3LYP	FREQ/ RB3LYP	RHF	B3PW91
C2—C3—C4—C5	0.76 (17)	0.54	0.76	0.35	0.59
C2—C3—C4—C9	179.76 (11)	179.82	179.77	179.76	179.76
C4—C3—C2—O3	174.17 (10)	176.27	174.15	177.03	176.33
C4—C3—C2—C1	2.54 (18)	0.87	2.55	0.74	1.06
C10—O3—C2—C3	113.77 (12)	112.31	113.74	108.57	112.94
C10—O3—C2—C1	−74.08 (13)	-72.01	-74.13	-74.91	-71.49
C1—O1—C5—C6	−177.98 (10)	179.64	-177.99	179.85	179.58
C1—O1—C5—C4	1.39 (17)	-0.07	1.43	0.08	-0.13
C9—C4—C5—O1	178.21 (10)	179.72	178.18	179.77	179.70
C3—C4—C5—O1	−2.74 (17)	-0.96	-2.76	-0.79	-1.08
C9—C4—C5—C6	−2.45 (18)	0.01	-2.43	0.00	0.00
C3—C4—C5—C6	176.61 (11)	179.34	176.63	179.45	179.22
C5—O1—C1—O2	−177.30 (11)	-177.89	-177.30	-178.35	-177.56
C5—O1—C1—C2	1.78 (16)	1.41	1.74	0.98	1.69
C3—C2—C1—O2	175.19 (12)	177.44	175.16	177.90	177.03
O3—C2—C1—O2	3.22 (18)	1.79	3.20	1.35	1.48
C3—C2—C1—O1	−3.81 (17)	-1.82	-3.79	-1.40	-2.16
O3—C2—C1—O1	−175.78 (9)	-177.46	-175.75	-177.95	-177.71
C5—C4—C9—C8	2.13 (18)	-0.01	2.17	1.46	-0.01
C3—C4—C9—C8	−176.87 (11)	-179.29	-176.84	-179.43	-179.18
O1—C5—C6—C7	−179.91 (11)	-179.73	-179.89	-179.77	-179.71
C4—C5—C6—C7	0.72 (19)	-0.02	0.70	0.00	-0.01
C2—O3—C10—O4	−1.43 (17)	-12.62	-1.35	-11.93	-12.64
C2—O3—C10—C11	179.59 (10)	167.64	179.61	168.55	167.65
C4—C9—C8—C7	−0.1 (2)	0.03	-0.21	0.03	0.03
C5—C6—C7—C8	1.4 (2)	0.03	1.34	0.00	0.02
C9—C8—C7—C6	−1.7 (2)	-0.03	-1.59	-0.02	-0.03

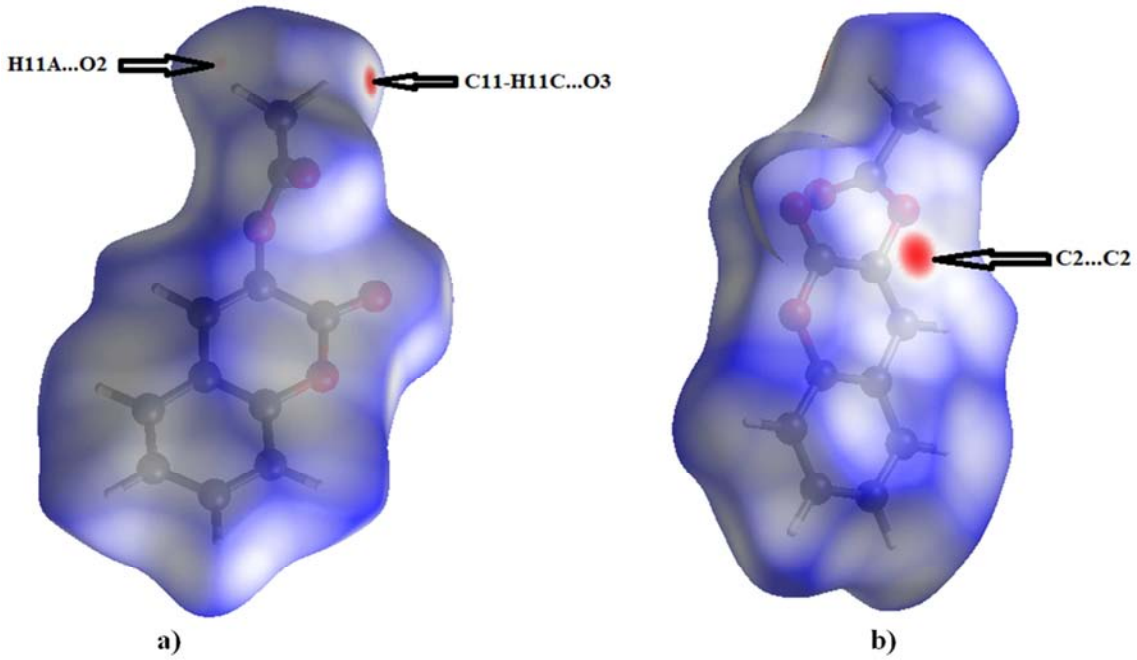

Figure 10. *Hirshfeld surfaces mapped over dnorm (-0.099 to 1.048 a.u.).*

3.3. Hirshfeld Surface Analysis

The Hirshfeld surface analysis of compound (I) was computed employing a standard (high) surface resolution with the three-dimensional (3D) d_{norm} surface schemed over a settled color scale of -0.099 (red) to 1.048 a.u. (blue). The resulting map shows two red tasks and one pale red task (negative d_{norm} values), highlighting distances less than the sum of the van der Waals radii. These short contacts indicate intermolecular C11—H11C…O3 (−x+1/2, y+1/2, z) hydrogen bond, C2…C2 (-x, 2-y, -z) and H11A…O2 (1/2-x,-1/2+y, z) interactions between the surface and the surroundings areas. The mapping also points out white tasks revealing distances almost equal to the sum of the van der Waals radii, and blue areas with distances greater than the sum of the van der Waals radii. The surfaces are made transparent in order to show the molecule (Figures 10a and

10b). Further, the colorful two-dimensional fingerprint (FP) plot is used to give information about the studied compound such as close contacts of atom pairs and the contributions from different contacts (figure 11). Hence, the blue tasks displayed near de=di ≃ 1.8–2.0 Å point out close C…C intermolecular contacts. The low contribution of these contacts (2.6%) to the total Hirshfeld surface area suggests the absence of π–π interactions [21] as forecasted by the crystallographic study. The most prominent type of contacts with 38.7% contribution to the overall surface contacts arises from H…O/O…H interactions. These are displayed on the left side as blue spikes with the tip at de + di=2.6 Å (Figure 11b), indicating O…H contacts. As generally found in organic chemistry, the H…H contacts have also a great contribution to Hirshfeld surface (28.7%). These interactions are displayed in the central area of the 2D- fingerprint characterized by a blue tip spike at de + di=2.4 Å (Figure 11c) while the C…H/H…C plot (20.2%) gives details on the intermolecular hydrogen bonds (Figure 11d). Other spots in the Hirshfeld surfaces indicating C… O / O… C and O… O contacts are observed with contributions of 7.8 and 2.0%, successively (Figures 11e and 11f).

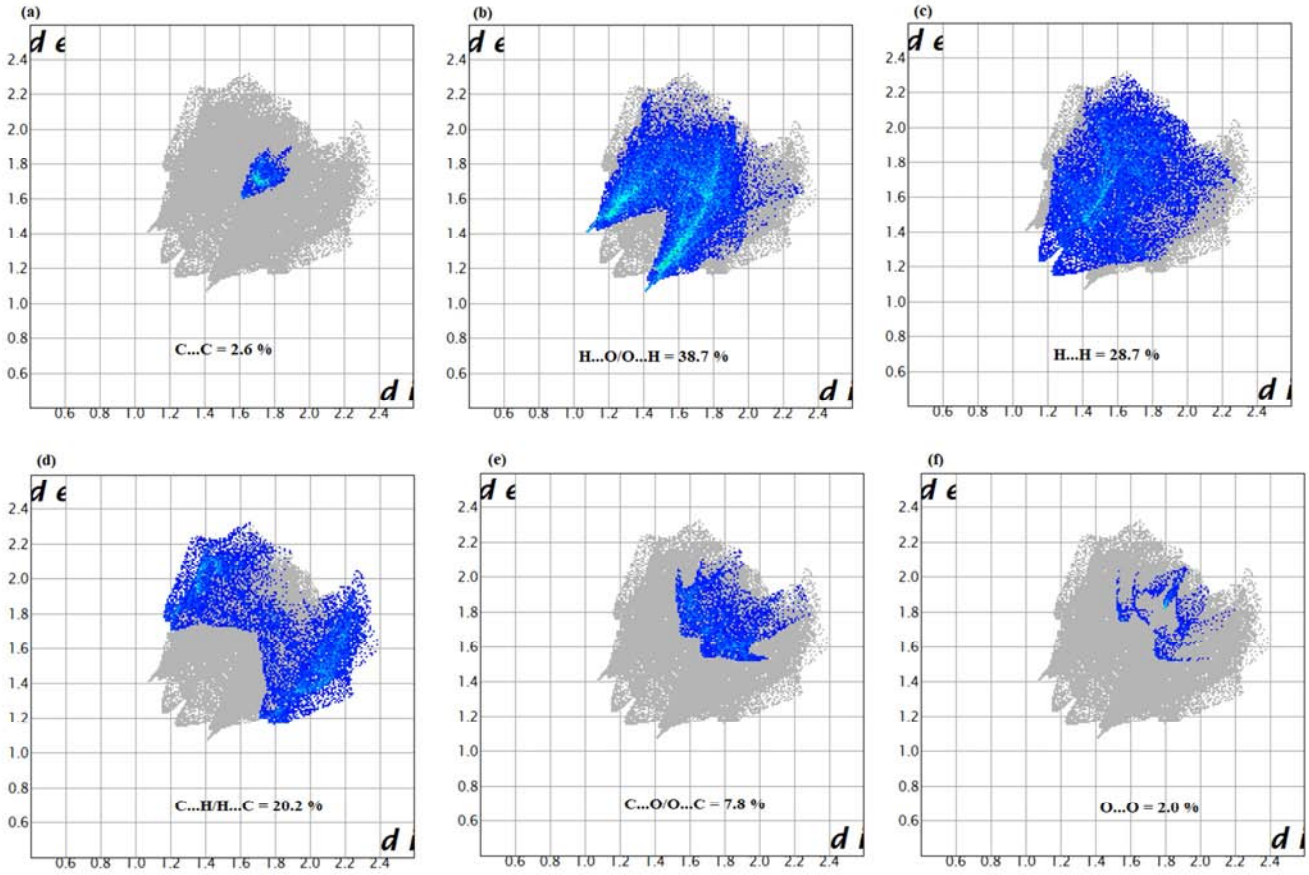

Figure 11. *Atom-atom interactions and their relative contribution to the Hirshfeld surface.*

Table 7. *Comparison of the observed and calculated stretching vibrational spectra of compound (I).*

Vibrational mode	Experimental IR, cm^{-1}	Calculated [B3LYP] 6-311^{++}G(d,p) scaled frequency, cm^{-1}
$\bar{\nu}_{C-H(aromatic)}$	3064	3162.82
$\bar{\nu}_{C=O(ester)}$	1776.7	1824.96
$\bar{\nu}_{C=O(lactone)}$	1731.8	1739.61
$\bar{\nu}_{C-O(ester)}$	1189.8	1140.07
$\bar{\nu}_{C-O(lactone)}$	1081.7	1091.01
$\bar{\nu}_{C=C(aromatic)}$	1607.4	1646.73

3.4. Theoretical Calculations

3.4.1. Comparison of Geometrical Parameters and Vibrational Frequencies

The molecular geometry evidenced by X-ray single crystal structure determination of (I) are compared to those obtained from Quantum Chemical Calculations. An inspection of the calculated bond lengths and bond angles reveals a strong correlation with the experiment values as judged by the root-mean-square deviation of 0.011 Å (DFT/RB3LYP), 0.016 Å (HF), 0.0004 Å (FREQ/RB3LYP) and 0.009 Å (B3PW91) for bond lengths and 0.5° (DFT/RB3LYP), 0.9° (RHF), 0.03° (FREQ/RB3LYP) and 0.5° (B3PW91) for bond angles

(Tables 4 and 5). These demonstrate that the method giving the best results is FREQ / RB3LYP and the ranking of these methods in descending order is FREQ / RB3LYP, B3PW91, DFT / RB3LYP and HF for bond lengths and bond angles. In addition, the computed torsion angles' analysis highlights the flatness of the coumarin ring system which is in good accordance with the crystallographic forecast, despite the difference observed in the torsion C2—O3—C10—O4 angle between this crystallography method (-1.43 (17)°) and the theoretical calculations ones (B3PW91, DFT / RB3LYP and HF) which generate values close to 12° (Table 6).

The theoretical spectrum (figure 13) was carried out using FREQ/RB3LYP/6-311G^{++}(d,p) method for optimizing geometries. Some vibrational modes assigned by Avogadro software [22] and their corresponding experimental values are summarized in Table 7. Comparison of the two set of data is performed with the statistic methods using the linear regression method. The coefficient of determination of the model established by calculated values vs experimental ones is very close to unity (R^2=0.9926) indicating a better fit for the model (figure 12). Thus, the model is suitable for predicting experimental infrared frequencies with very good precision.

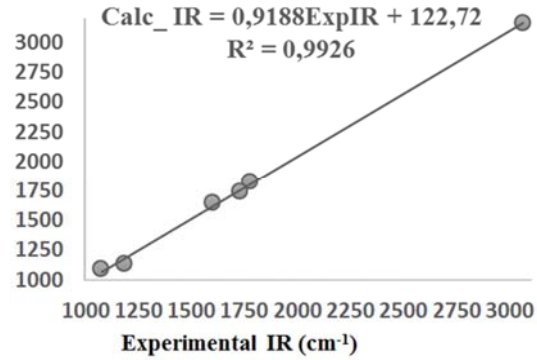

Figure 12. *Correlation graphic between the experimental and theoretical vibration frequencies of compound (I) (cm^{-1}).*

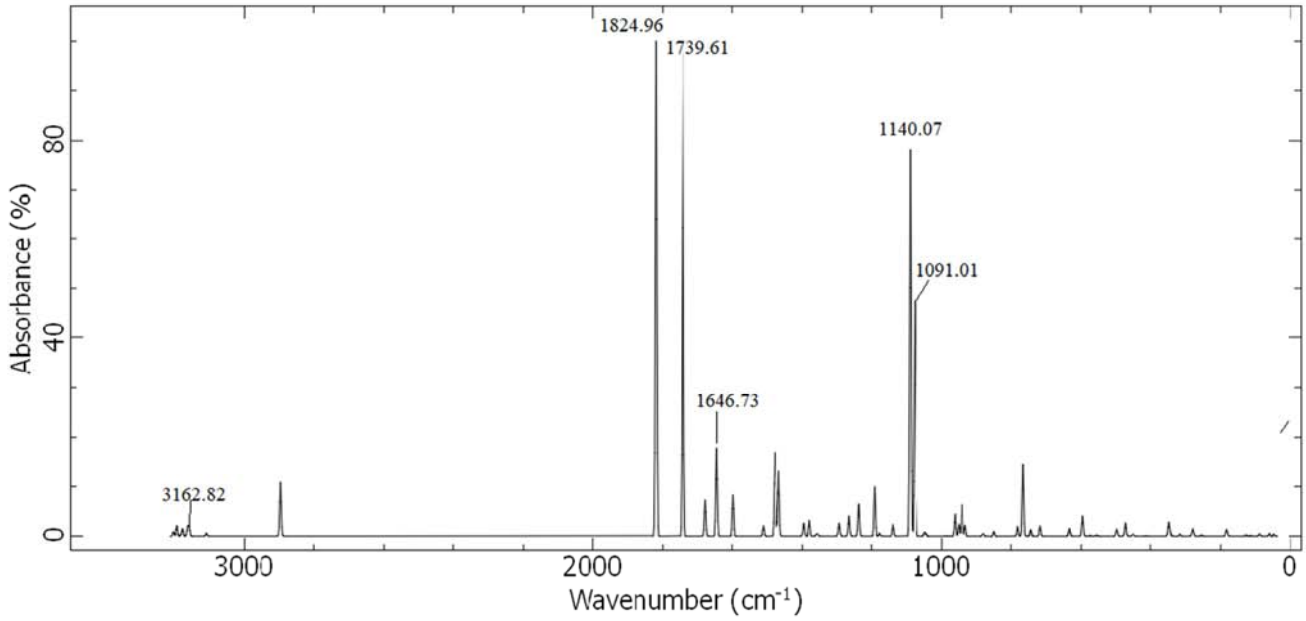

Figure 13. *Computed vibrational spectrum.*

3.4.2. Molecular Electrostatic Potential (MEP)

The molecular electrostatic potential (MEP) is an electrostatic function derived from Coulomb forces that describes the interactions between electrons and the nuclear charges. It plays important role in inspecting reactivity since an approaching electrophile will be attracted into negative sites.

It is defined in atomic units, a.u, as follows [23, 24]:

$$V(r) = \sum_A \frac{Z_A}{|R_A - r|} - \int \frac{\rho(r')}{|r' - r|} d^3r' \qquad (1)$$

where Z_A is the charge of nucleus A sited at R_A, $\rho(r')$ is the electronic density function of the molecule, and r' is the dummy integration variable.

In this study, we have calculated MEP with optimized geometries from DFT / RB3LYP, RHF, FREQ / RB3LYP and B3PW91 methods utilizing the 6-311^{++}G (d, p) basis set to supply information with respect to these reactive sites to distinguish the electrophilic and nucleophilic areas. The outcomes of these calculations are presented in color visualizations (Figure 14). In this figure, the red color in the figure indicates areas of higher negative potential which are favorable for electrophilic attack, while the blue color (higher positive potential) identifies beneficial sites for nucleophilic attack. In Figure 14, two possible areas on compound (I) for electrophilic attack are discernible indicating negative sites. These regions are situated on O2 and around O3 and O4 oxygen atoms with maximum values of -0.0552, -0.0583, -0.0608 and -0.0606 a.u. for DFT/RB3LYP, FREQ/RB3LYP, RHF and B3PW91 methods, respectively. Therefore, Figure 14 corroborates the presence of the intermolecular C11–

H11C…O3 interaction.

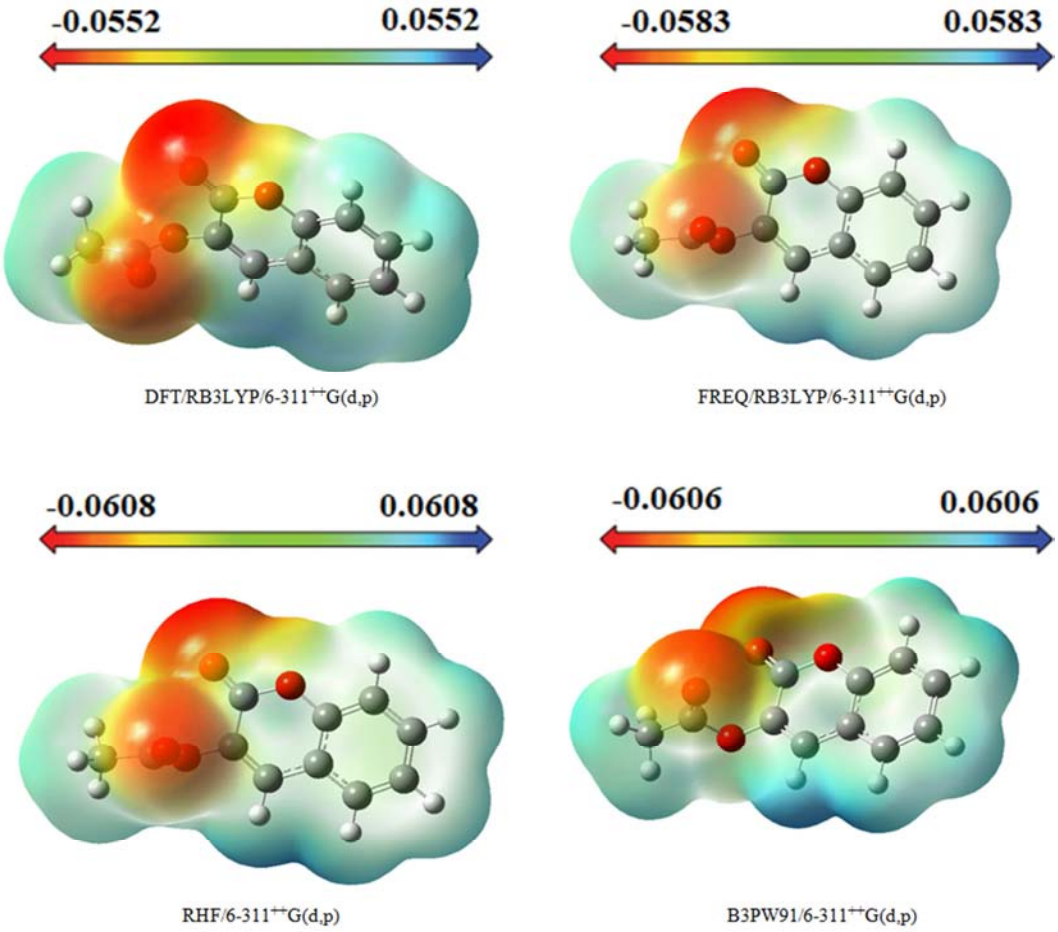

Figure 14. *Molecular electrostatic potential map (MEP) (in a.u.) calculated at DFT/RB3LYP, FREQ/RB3LYP, RHF and B3PW91 level frontier molecular orbitals analysis with 6-311^{++}G(d,p) basis set.*

3.4.3. HOMO-LUMO Analysis

The outcomes of the apportionments and energy levels of the topmost occupied molecular orbital (HOMO) and the unoccupied molecular orbital (LUMO) calculated using four quantum chemical methods are depicted in figure 15. The computations disport that compound (I) possesses 53 occupied molecular orbitals and the energy gap between the LUMO and HOMO levels are 4.574 (DFT/B3LYP), 4.627 (FREQ/ B3LYP), 4.606 (B3PW91) and 9.858 eV (RHF), successively. The first three computational results of HOMO-LUMO gaps (DFT/B3LYP, FREQ/ B3LYP, B3PW91 methods) in the range 4.574-4.627 eV demonstrate that 2-oxo-2H-chromen-3-yl acetate is polarizable together with a high chemical reactivity and low kinetic stability and is also called soft molecule [25]. The latter value (ΔE =9.858 eV), almost double the previous ones could suggest that RHF method is not suitable for estimating energy gap between the LUMO and HOMO levels. The HOMO and LUMO energies, the energy gap (ΔE), the ionization potential (I), the electron affinity (A), the absolute electronegativity (χ), the absolute hardness (η), the softness (S) and the optimization energy (E) for the studied compound have been estimated and the outcomes are displayed in Table 8. By utiltzing HOMO and LUMO energy values for a molecule, electronegativity and chemical hardness can be expressed as follows [26]:

$$\chi = -(E_{HOMO} + E_{LUMO})/2 \quad (2)$$

$$\eta = (E_{LUMO} - E_{HOMO})/2 \quad (3)$$

$$S = 1/2\eta \quad (4)$$

$$I = -E_{HOMO} \quad (5)$$

$$A = -E_{LUMO}. \quad (6)$$

$$\Delta E = E_{LUMO} - E_{HOMO} \quad (7)$$

Table 8. *The computed chemical properties of (I) using 6-311^{++}G(d,p) basis set.*

	DFT/ B3LYP	FREQ/ B3LYP	RHF	B3PW91
E_{LUMO} (eV)	-2.305	-2.277	0.855	-2.303
E_{HOMO} (eV)	-6.879	-6.904	-9.003	-6.909
I (eV)	6.8879	6.904	9.003	6.909
A (eV)	2.305	2.277	-0.855	2.303
χ (eV)	4.59	4.59	4.07	4.61
η (eV)	2.29	2.31	4.93	2.30
S (eV^{-1})	0.22	0.22	0.10	0.22
ΔE (eV)	4.574	4.627	9.858	4.606
E (au)	-725.10	-724.95	-720.86	-724.81

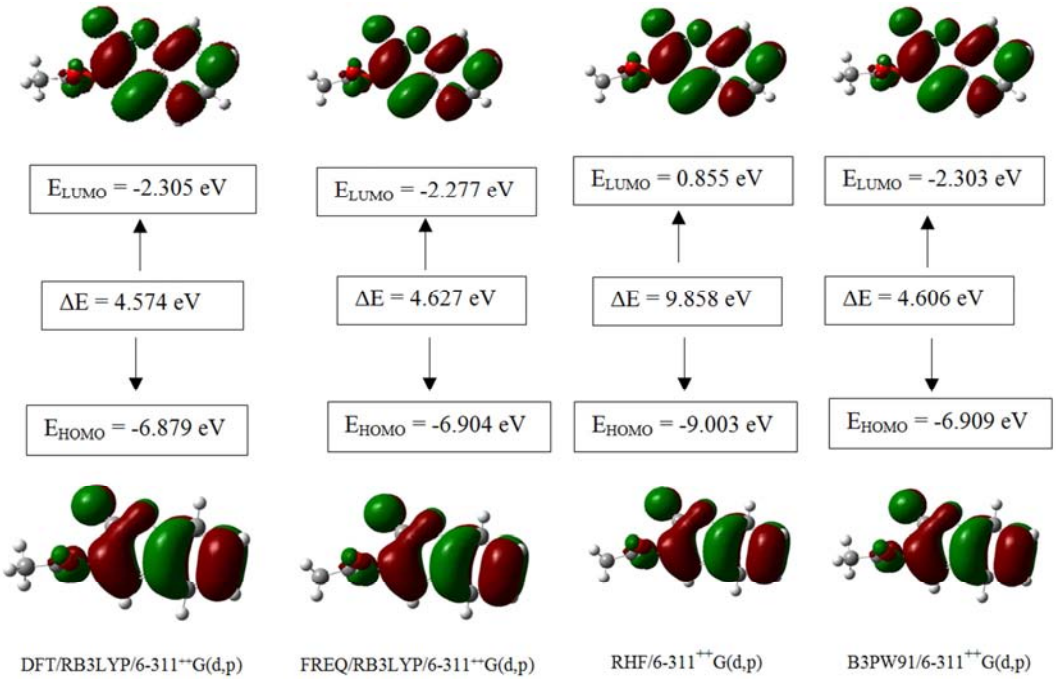

Figure 15. *The distributions and energy levels of the HOMO and LUMO orbitals computed for compound (I).*

Table 9. *Computed Mulliken atomic charges utilizing 6-311^{++}G(d,p) basis set.*

Atom	DFT/RB3LYP	FREQ/RB3LYP	RHF	B3PW91
O1	-0.107	-0.123	-0.272	-0.054
O2	-0.271	-0.278	-0.366	-0.260
O3	-0.016	-0.029	-0.103	-0.039
O4	-0.196	-0.207	-0.281	-0.178
C1	0.616	0.585	0.912	0.730
C2	-0.559	-0.718	-862	-0.876
C3	0.165	0.517	0.752	0.727
H3	0.199	0.170	0.248	0.238
C4	2.32	1.934	1.543	1.990
C5	-1.961	-1.905	-2.088	-2.363
C6	-0.407	-0.367	-0.187	0.210
H6	0.210	0.182	0.245	0.177
C7	-0.348	-0.253	-0.364	-0.251
H7	0.175	0.141	0.215	0.209
C8	-0.137	-0.048	-0340	-0.409
H8	0.174	0.140	0.203	0.216
C9	-0.112	0.018	0.330	-0.450
H9	0.140	0.105	0.185	0.246
C10	0.084	0.041	0.238	0.068
C11	-0.510	-0.354	-0.543	-0.619
H11A	0.174	0.147	0.167	0.190
H11B	0.169	0.150	0.171	0.195
H11C	0.199	0.153	0.197	0.226

3.4.4. The Mulliken Charge Population

Mulliken charges originate from the Mulliken population examination and give a means of evaluating partial nuclear charges from calculations carried out by the methods of computational chemistry. These atomic charges affect a lot of properties of molecular systems such as dipole moment, molecular polarizability, electronic structure, and so on. The charge distributions calculated by the Mulliken method [27-30] for optimized geometry of compound (I) is summarized in table 9. The calculated charge of O2 oxygen atom is negative and that of the carbon atom C10 is positive for all methods used (table 9). The resulting electrostatic interactions between them are materialized by the short intramolecular C10…O2 bond in the solid state (figure 8). Further, the charges of the three atoms (C11;H11C;O3) extracted from table 9 are (-0.510 e; 0.199 e;-0.016 e), (-0.354 e; 0.153 e; -0.029 e), (-0.543e; 0.197 e; -0.103 e) and (-0.619 e; 0.226 e; -0.039 e) for the DFT/RB3LYP/6-311^{++}G(d,p), FREQ/RB3LYP/6-311^{++}G(d,p), RHF/6-311^{++}G(d,p) and B3PW91/6-311^{++}G(d,p) methods, respectively. These values highlighting interactions between H11C and O3 atoms confirm the intermolecular hydrogen bond C11–H11C…O3[−x+1/2, y+1/2, z]. Likewise, the computed Mulliken charges of C7 and C8 are negatives pointing out that these carbon atoms are electronegatives. Thus, they can establish other hydrogen bonds in the gaseous state.

3.4.5. Non-linear Optical Properties

Since the discovery of nonlinear optical (NLO) phenomenon for the first time in 1961, nonlinear optical frequency conversion materials have played major role in many fields, such as optical communication, laser technology, optical data storage, optical information processing, image manipulation etc [31 32]. The very first material used to exploit for their nonlinear optical (NLO) properties was potassium dihydrogen phosphate (KDP). It was used in the first experiments in nonlinear optics and is still used widely in nonlinear optics devices.

Currently, Urea is used to replace KDP due to its second harmonic efficiency which is three times higher than that of the KDP crystals [33].

At present, because of potential applications in various fields, a huge number of investigate papers in new materials

indicating effective nonlinear optical properties have been of awesome interest [34-38]. So, the use of quantum chemical methods such as density functional theory (DFT), Hartree-Fock (HF) and B3PW91 for molecular hyperpolarizabilities is awaited to supply a supervision and accelerate upcoming experimental studies [39, 40].

Hence, within the display job, we have minimized the geometries with GAUSSIAN-09W program package [16] at DFT / RB3LYP, RHF and B3PW91methods using 6-311^{++}G (d, p) basis set and computed the dipole moments (μ), the polarizabilities (<α>), the anisotropy of the polarizabilities (<Δα>) and the first-order hyperpolarizabilities (β) which gives information about the material capability to generate second order non-linear effects [41]. These parameters are defined as [42-43]:

$$\mu = \left(\mu_x^2 + \mu_y^2 + \mu_z^2\right)^{\frac{1}{2}} \quad (8)$$

$$\langle\alpha\rangle = \frac{\alpha_{xx}+\alpha_{yy}+\alpha_{zz}}{3} \quad (9)$$

$$\langle\Delta\alpha\rangle = \left[\frac{(\alpha_{xx}-\alpha_{yy})^2+(\alpha_{yy}-\alpha_{zz})^2+(\alpha_{zz}-\alpha_{xx})^2+6(\alpha_{xy}^2+\alpha_{xz}^2+\alpha_{yz}^2)}{2}\right]^{\frac{1}{2}} \quad (10)$$

$$\beta = \left[\left(\beta_{xxx}+\beta_{xyy}+\beta_{xzz}\right)^2 + \left(\beta_{yyy}+\beta_{yzz}+\beta_{yxx}\right)^2 + \left(\beta_{zzz}+\beta_{zxx}+\beta_{zyy}\right)^2\right]^{\frac{1}{2}} \quad (11)$$

All the numerical outcomes of the tensors regarding the polarizability were expressed to electronic units (esu) and recorded in Tables 10, 11 and 12, with (α: 1 a.u.=0.1482 x10^{-24} esu; β: 1 a.u.=8.6393x10^{-33} esu) [44].

Table 10. *Computed dipole moment (D) using the 6-311^{++}G(d,p) basis set.*

	μ_x	μ_y	μ_z	<μ >
DFT/RB3LYP	2.2716	-3.8227	-1.4063	4.6638
RHF	2.3609	-4.0474	-1.6281	4.9604
B3PW91	2.2120	-3.7658	-1.3740	4.5785

Table 11. *All α ×10^{-24} (esu) components, <α> ×10^{-24} (esu) and <Δα> ×10^{-24} (esu) values computed with the 6-311^{++}G(d,p) basis set.*

	α_{xx}	α_{xy}	α_{yy}	α_{xz}	α_{yz}	α_{zz}	<α>	<Δα>
DFT/RB3LYP	9.81	0.80	12.71	0.80	0.28	13.74	12.09	4.07
RHF	-9,80	0,81	-12,72	0,87	0,36	-13,88	12.07	4.18
B3PW91	9,65	0,8	12,51	0,74	0,28	13,62	11.93	4.05

Table 12. *First-order hyperpolarizabilities (β) values of (I) computed with DFT, HF and B3PW91 methods.*

	β_{xxx} (a.u)	β_{yyy} (a.u)	β_{zzz} (a.u)	β_{xyy} (a.u)	β_{xxy} (a.u)	β_{xxz} (a.u)	β_{xzz} (a.u)	β_{yzz} (a.u)	β_{yyz} (a.u)	β_{xyz} (a.u)	β×10^{-30} (esu)
DFT/RB3LYP	-35,02	-21,93	-6,21	11,07	-10,02	-4,71	-5,49	9,91	1,59	0,65	0.3278
RHF	-36,10	-24,70	-6,586	11,24	-9,55	-4,30	-6,43	8,10	0,75	0,07	0.3630
B3PW91	-34,09	-21,49	-6,04	11,55	-10,13	-3,85	-6,12	6,63	1,6	0,84	0.3362

For investigation, urea molecule with its parameters (<μ >=1.37D, <α>=3.83x10^{-24} esu [45-47], and <β >=0.1947x10^{-30} esu [48]) is utilized for comparison in the study of NLO properties of compound (I). As can be famous from tables (10-12), the values of all parameters for (I) are somewhat higher than those of the urea molecule.

For additional subtleties, the dipole moments of compound (I) originating from the DFT / B3LYP, HF and B3PW91 calculations are 3.40, 3.62 and 3.34 times higher than that of the urea molecule, respectively (Table 10). Similarly, the calculated first-order hyperpolarizabilities are also 1.68, 1.86 and 1.73 times higher than that of the urea molecule. In addition, the estimated values of the average linear polarizability <α> are close to that of the urea molecule, i.e. 1.06 (DFT / B3LYP), 1.09 (HF) and 1.06 (B3PW91) (table 11).

These values demonstrate a favorable first order hyperpolarizability of 2-oxo-2H-chromen-3-yl acetate which can generate second order non-linear effects. Therefore, 2-oxo-2H-chromen-3-yl acetate can be considered a potential candidate having nonlinear optical effects and may have potential applications in the development of NLO materials.

4. Conclusion

In ouline, we began our study with the synthesis of the structure and characterized it by spectrometry and by X-ray crystallography. Also, we have inspected its intermolecular interactions by means of Hirshfeld surface analysis.

Then the estimated geometric parameters and infrared spectrum originating from quantum chemical calculations are compared respectively with the x-ray crystal determination data and the experimental IR spectrum. In this comparison, we can notice that there are no notable differences except the experimental torsion angle, C2—O3—C10—O4, which differs from the calculated values by around 12°. Moreover, molecular electrostatic potential, HOMO-LUMO examination and the Mulliken charge population of 2-oxo-2H-chromen-3-yl acetate have been explored utilizing DFT/RB3LYP, FREQ/RB3LYP, HF and B3PW91 calculations outcomes. The generated MEP maps indicate the areas of negative potential which are located around electronegative atoms i.e oxygen atoms and the positive potential which is located around the hydrogen

atoms. These regions highlight the areas from where the compound can establish intra- and intermolecular interactions.

Additionally, Mulliken charges computed in the gaseous state show partial negative charges on atoms O2, O3, C11 and partial positive charges on H11C, C10 confirming the intermolecular hydrogen bond C11–H11C…O3[−*x*+1/2, *y*+1/2, *z*] and the short intramolecular C10…O2 bond.

Endly, the calculated values of the first-order hyperpolarizabilities (β) with DFT/B3LYP, HF and B3PW91 methods have suggested non-linear optical properties of the studied compound.

Supplementary Materials

CCDC-2052679 contains the supplementary crystallographic data for this paper. These data can be obtained free of charge via https://www.ccdc.cam.ac.uk/structures/, or by e-mailing data_request@ccdc.cam.ac.uk, or by contacting The Cambridge Crystallographic Data Centre, 12 Union Road, Cambridge CB2 1EZ, UK; fax: +44(0)1223-336033.

Conflicts of Interest

The authors declare that they have no conflict of interest.

Acknowledgements

The authors offer their thanks to the Spectropole Service of the Federation of Chemical Sciences (Aix-Marseille University, France) for the spectroscopic investigation.

References

[1] Yu, D.; Suzuki, M.; Xie, L.; Morris-Natschke, S. L. & Lee, K.-H.; (2003) *Med. Res. Rev.* 23, 322–345.

[2] Yu, D.; Morris-Natschke, S. L. & Lee, K.-H.; (2007) *Med. Res. Rev.* 27, 108–132.

[3] Abernethy, J. L.; (1969). *J. Chem. Educ.* 46, 561–568.

[4] Vukovic, N.; Sukdolak, S.; Solujic, S. & Niciforovic, N.; (2010) *Arch. Pharm. Res.* 33, 5–15.

[5] Wang, M.; Wang, L.; Li, Y. & Li, Q.; (2001) *Transition Met. Chem.* 26, 307–310.

[6] Basanagouda, M.; Kulkarni, M. V.; Sharma, D.; Gupta, V. K.; Pranesha, P.; Sandhyarani, P. and Rasal V. P.; (2009) *J. Chem. Sci.*, 121, 485–495.

[7] Emmanuel-Giota, A. A.; Fylaktakidou, K. C.; Litinas, K. E.; Nicolaides, D. N. and Hadjipavlou-Litina, D. J.; (2001) *Heterocycl. Chem.*, 38, 717–722.

[8] Abou, A.; Djandé, A.; Kakou-Yao, R.; Saba, A. and Tenon, A. J.; (2013) *Acta Cryst.,* E69, o1081–o1082.

[9] Ouédraogo, M.; Abou, A.; Djandé, A.; Ouari, O. and Zoueu, T. J.; (2018) *Acta Cryst.*, E74, 530–534.

[10] Rigaku, OD.; (2015) *CrysAlis PRO*. Rigaku Oxford Diffraction, Yarnton, England.

[11] Burla, M. C.; Caliandro, R.; Carrozzini, B.; Cascarano, G. L.; Cuocci, C.; Giacovazzo, C.; Mallamo, M.; Mazzone, A. and Polidori, G., *J.;* (2015) *Appl. Cryst.*, 48, 306–309.

[12] Farrugia, L. J.; (2012) *J. Appl. Cryst.*, 45, 849–854.

[13] Sheldrick, G. M.; (2015) *Acta Cryst.*, C71, 3–8.

[14] Spek, A. L.; (2009) *Acta Cryst.*, D65, 148–155.

[15] Wolff, S. K.; Grimwood, D. J.; McKinnon, J. J.; Turner, M. J.; Jayatilaka, D. and Spackman, M. A.; (2012) *Crystal Explorer.* The University of Western Australia.

[16] Frisch, M. J.; Trucks, G. W.; Schlegel, H. B.; Scuseria, G. E.; Robb, M. A.; Cheeseman, J. R.; et al.; (2013) GAUSSIAN09. Gaussian, Inc., Wallingford, CT, USA.

[17] Allen, F. H.; Walson, D. G.; Orpen, A. G.; Taylor, R.; (1987) *J. Chem. Soc., Perkin Trans. II*, S1-S9.

[18] Gomes, L. R.; Low, J. N.; Fonseca, A.; Matos, M. J. and Borges, F.; (2016) *Acta Cryst.*, E72, 926–932.

[19] Ziki, E.; Yoda, J.; Djandé, A.; Saba, A. and Kakou-Yao, R.; (2016) *Acta Cryst.*, E72, 1562–1564.

[20] Cremer, D. & Pople, J.; (1975). J. Am. Chem. Soc. 97, 1354–1358.

[21] Bitzer, S. R.; Visentin, C. L.; Hörner, M.; Nascimento, M. A. C. and Filgueiras, C. A. L.; (2017) *J. Mol. Struct.*, 1130, 165–173.

[22] Hanwell, M. D.; Curtis, D. E.; Lonie, D. C.; Vandermeersch, T.; Zurek, E. and Hutchison, G. R.; (2012) *Journal of Cheminformatics, 4 (1), 17.*

[23] Murray, J. S.; Politzer, P.; The electrostatic potential: an overview. *WIREs Comp Mol Sci*, 2011, 1: 153–163

[24] Politzer, P. and Murray, J. S.; (2002) *Theoretical Chemistry Accounts*, 108 (3), 134–142.

[25] Fleming, I.; (1976) *Frontier Orbitals and Organic Chemical Reactions*, John Wiley & Sons, London, UK.

[26] Pearson, R. G.; (1986) *Proceedings of the National Academy of Sciences of the United States of America*, 83 (22), 8440–8841.

[27] Mulliken, R. S.; (1955) *The Journal of Chemical Physics*, 23 (10), 1833–1840.

[28] Mulliken, R. S.; (1955) *The Journal of Chemical Physics*, 23 (10), 1841–1846.

[29] Mulliken, R. S.; (1955) *The Journal of Chemical Physics*, 23 (12), 2338–2342.

[30] Mulliken, R. S.; (1955 *The Journal of Chemical Physics*, 23 (12), 2343–2346.

[31] Janarthanan, S.; Samuel, R. S.; Rajan, Y. C.; Pandi, S.; J. Therm. Anal. Calorim., 2012, 107, 1213-1217.

[32] Bhagavannarayana, G.; Riscob, B.; Mohd, S.; Mater. Chem. Phys., 2011, 126, 20-23.

[33] Gomes, E. D.; Venkatraman, V.; Nogueira, E.; Belsley, M.; Garrido, S. P.; Mater Syn., 2000, 115, 225–228).

[34] Zhang, R.; Du, B.; Sun, G. and Sun, Y.; (2010) *Spectrochimica Acta A*, vol. 75, no. 3, pp. 1115–1124.

[35] Yazıcı, S.; Albayrak,.; Gümrükçüolu, I.; enel, I. and Büyükgüngör, O.; (2011) *Journal of Molecular Structure*, vol. 985, no. 2-3, pp. 292–298.

[36] Chemia, D. S. and Zyss, J.; *Non Linear Optical Properties of Organic Molecules and Crystal*, Academic Press, New York, NY, USA, 1987.

[37] Zyss, J.; *Molecular Non Linear Optics*, Academic Press, Boston, Mass, USA, 1994.

[38] Ben Ahmed, A.; Feki, H.; Abid, Y. and Minot, C.; (2010) *Spectrochimica Acta A*, vol. 75, no. 4, pp. 1315–1320.

[39] Suponitsky, K. Y.; Tafur, S; Masunov, A. E.; (2008) *Journal of Chemical Physics*, 129, 044109-11.

[40] Avci, D.; Başoğlu, A.; Atalay, Y.; (2011) *International Journal of Quantum Chemistry*, 111, 1, 130-147.

[41] Machado, A. E. H.; Neto, N. M. B.; Ueno, L. T.; et al.; (2008) *Journal of Photochemistry Photobiology A-Chemistry*, 199, 1, 23–33.

[42] Abraham, J. P.; Sajan, D.; Hubert, Joe I. H. and Jayakumar, V. S.; (2008) *Spectrochimica Acta Part A*, 71, 2, 355-367.

[43] Karamanis, P.; Pouchan, C. and Maroulis, G.; (2008) *Physical Review A*, 77, 013201-013208.

[44] Ben Ahmed, A.; Feki, H.; Abid, Y.; Boughzala, H. and Mlayah, A.; (2008) *Journal of Molecular Structure*, 888, 1-3, 180-186.

[45] Nkungli, N. K.; Ghogomu, J. N.; (2016) J. *Theor. Chem.*, 2016, 1–19.

[46] Pluta, T.; Sadlej, A. J.; (2001) J. *Chem. Phys.*, 114, 136.

[47] Song, X.; Farwell, S. O.; (2004) *J. Anal. Appl. Pyrolysis*, 71, 901–915.

[48] Eme, A.; Günedodu Sadinç, S.; (2014) *BAÜ Fen Bil. Enst. Dergisi Cilt* 16 (1) 47-75.